Relationship Quantification of Image Degradations

Boyun Li, Yuanbiao Gou, Wenxin Wang, Peng Hu, Wangmeng Zuo, and Xi Peng

***Abstract*—In this paper, we study two challenging but less-touched problems in image restoration, namely, i) how to quantify the relationship between image degradations and ii) how to improve the performance of a specific restoration task using the quantified relationship. To tackle the first challenge, we propose the Degradation Relationship Index (DRI), which is defined as the mean drop rate difference in validation loss between two models, where one trained solely with anchor degradation and the other trained with both anchor and auxiliary degradations. By quantifying degradation relationship using DRI, we reveal that i) a positive DRI consistently indicates performance improvement when a beneficial auxiliary degradation is incorporated during training; ii) the proportion of auxiliary degradation is crucial to the anchor task performance. In other words, performance improvement is achieved only when the anchor and auxiliary degradations are combined in an appropriate proportion. Based on these observations, we further propose a simple yet effective Degradation Proportion Determination (DPD) method to estimate whether a given degradation combinations can enhance performance on the anchor restoration task with the assistance of auxiliary degradation. Extensive experimental results verify the effectiveness and generalizability of our method on noise, rain streak, haze and snow.**

***Index Terms*—Image restoration, relationship quantification, image degradation.**

I. Introduction

IN THE real world, images are often contaminated by various degradations such as noise, rain, haze, and snow, thus deteriorating the imaging quality and making difficulty for downstream tasks. To obtain visually pleasant images, plentiful works have been conducted and significant advancements have been achieved during past years [10], [17], [18], [25], [27], [37], [41], [43], [44], [45], [46], [47], [48].

Although these methods perform well by designing models tailored to specific degradation, they are less attractive to some real-world scenarios such as autopilot, where handling multiple degradations with a unified model is highly desirable. To develop such an all-in-one model, several studies have been conducted for implicit [13], [36] or explicit restoration [2], [16] by introducing novel network architectures, objective function, or training strategy. Although promising results have been achieved, these works primarily focus on removing multiple degradations from inputs, largely overlooking another important and promising direction, i.e., Relationship Quantification of Image Degradations (RQID). Motivated by the observations that training with multiple degradations results in performance improvements for some degradations while deterioration for others [13], this paper explores how to mathematically quantify such performance variation. Specifically, the primary goal of RQID is to develop a quantification tool that can reflect the positive or negative influence of given auxiliary degradation on the anchor restoration task, thereby improving the performance on anchor task when beneficial auxiliary degradations are introduced.

To achieve RQID, in this paper, we propose the Degradation Relationship Index (DRI) to quantitatively answer how the performance of a given anchor restoration task (e.g., dehazing) will be influenced when another type of degraded images (e.g., noisy images) is introduced into the training process. Specifically, DRI is designed to quantify the relationship between the anchor and auxiliary degradations. It is defined as the mean drop rate difference in the validation loss between two models, where one trained solely with the anchor degradation and the other trained with both anchor and auxiliary degradations. As shown in Fig. 1, a positive DRI consistently indicates performance improvement on the anchor restoration task, a conclusion further supported by subsequent analysis and experiments. Back to the figure, compared to the baseline (triangles), the model with a positive DRI (circles) converges faster and achieves better performance, highlighting the positive influence of the auxiliary degradation. In contrast, the model with a negative DRI (crosses) converges slower and performs worse, reflecting the detrimental impact of the given auxiliary degradation. Interestingly, the only difference between the models represented by circles and crosses lies in the proportion of the auxiliary degradation. This suggests that the degradation combination, including both the degradation type and proportion, plays a critical role in determining image restoration performance. Specifically, the performance of the anchor restoration task improves only when degradations are combined in appropriate proportions. Based on this observation

Received 21 March 2024; revised 11 March 2025; accepted 29 April 2025. Date of publication 9 May 2025; date of current version 3 July 2025. This work was supported in part by the National Key R&D Program of China under grant 2024YFB4710604, in part by the NSFC under Grant 62176171, Grant 62472295, and Grant U24B20174, in part by the Fundamental Research Funds for the Central Universities under Grant CJ202303 and Grant CJ202403, in part by Sichuan Science and Technology Planning Project under Grant 24NSFTD0130, and in part by the TCL science and technology innovation fund. Recommended for acceptance by L. Zhang. *(Boyun Li and Yuanbiao Gou contributed equally to this work.) (Corresponding author: Xi Peng.)*

Boyun Li, Yuanbiao Gou, Wenxin Wang, and Peng Hu are with the College of Computer Science, Sichuan University, Chengdu 610065, China (e-mail: liboyun.gm@gmail.com; gouyuanbiao@gmail.com; wangwenxin.gm@gmail.com; penghu.ml@gmail.com).

Wangmeng Zuo is with the School of Computer Science and Technology, Harbin Institute of Technology, Harbin 150001, China (e-mail: wmzuo@hit.edu.cn).

Xi Peng is with the College of Computer Science and National Key Laboratory of Fundamental Algorithms and Models for Engineering Numerical Simulation, Sichuan University, Chengdu 610065, China (e-mail: pengx.gm@gmail.com).

The code is available at https://github.com/XLearning-SCU.

This article has supplementary downloadable material available at https://doi.org/10.1109/TPAMI.2025.3568690, provided by the authors.

Digital Object Identifier 10.1109/TPAMI.2025.3568690

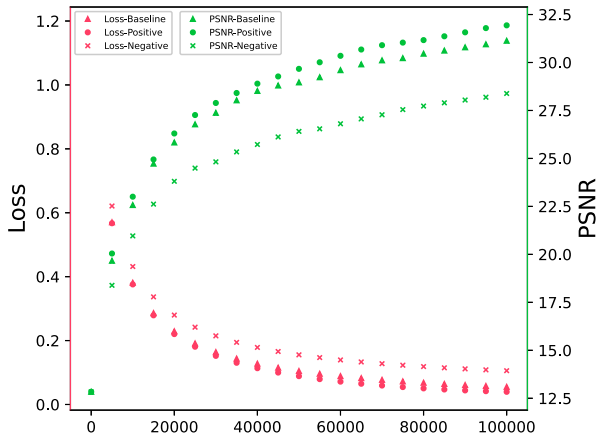

Fig. 1. Our observation and the effectiveness of DRI. As a baseline, the red and green triangles illustrate the validation loss and PSNR of the model trained on the anchor degradation (e.g., haze). Achieving better and worse restoration performance respectively, the circles and crosses are the models trained with both anchor and auxiliary degradations (e.g., noise), where the only difference between them is the proportion of the auxiliary degradation (10% and 50% noise for positive and negative degradations, respectively).

and leveraging DRI as a metric, we introduce Degradation Proportion Determination (DPD), a simple yet effective method designed to identify whether given degradation combinations can enhance performance on the anchor restoration task. Notably, DRI is significantly different from conventional task affinity methods [6], [42] in two aspects. First, DRI is compatible with all loss functions and network architectures, whereas most existing task affinity methods require specifically designed network structures. Second, DRI demonstrates strong predictability on indicating how auxiliary degradations influence anchor restoration performance, while existing task affinity methods fail to reliably anticipate such effects in image restoration tasks as validated in Section IV-D.

To summarize, the contributions and novelties of this study are as below:

- To the best of our knowledge, this work might be one of the first attempt to systematically explore and exploit the relationship between different degradations.
- We introduce DRI, a predictable and flexible solution to quantify the relationship between two given degradations, specifically assessing how the performance of the anchor restoration task will be influenced by introducing a auxiliary degradation into the training process.
- To address the lack of a benchmark for this emerging topic, we construct a novel benchmark, dubbed RESIDE+. By leveraging RESIDE+, RQID methods can be largely immune to the influence of content discrepancy and concentrate on the degradations relationship. Extensive experiments verify the effectiveness and generalizability of proposed method.

II. Related Work

This section will briefly review two related topics, namely, the all-in-one restoration (multiple degradations restoration, MDR) and image deweathering.

A. Multiple Degradations Restoration

To handle multiple degradations commonly seen in the real-world scenarios, a large number of MDR methods [2], [4], [13], [16], [22], [36] have been proposed to handle different degradations with a single model. Although significant advancements have been achieved, most efforts concentrate on designing novel network architectures, objective functions or training strategies, whereas they overlook the exploration and analysis of phenomena concomitant with MDR, such as performance variations induced by other degradations, i.e., RQID.

Different from the aforementioned studies on MDR, this work does not attempt to develop a new image restoration method. Instead, it aims to develop a RQID tool to study and leverage the degradation relationship. It is worth noting that although previous works [16], [28] introduce data augmentation methods using additional degradations to promote target task performance, our work present two advantages. First, our studies present a quantifiable paradigm to assess the influence of auxiliary degradations, enabling us to systematically determine the optimal degradation without relying on exhaustive trial-and-error experimentation. Second, our method eliminates the need for costly synthesis procedures by directly replacing the original images with versions containing auxiliary degradations. This makes our method highly compatible with a wide range of degradations, including complex ones like haze, which are often expensive to generate in traditional data augmentation pipelines. In summary, instead of proposing another ad-hoc data augmentation method, our work establishes a paradigm to bridge the gap between task-specific data augmentation and a more fundamental understanding of degradation interactions. By doing so, we reduce the reliance on extensive trial-and-error experiments, leading to considerable savings in computational resources and synthesis costs.

B. Image Deweathering

Image deweathering [13], [16], [26], [28], [34], [35], [36], [49] aims to remove adverse weather (such as rain streak, haze and snow) to produce visually appealing results for users. Without loss of generality, we take image dehazing, deraining and desnowing as examples to investigate the RQID. Image dehazing aims to restore the scene radiance from the observed hazy images [1], [5], [8], [11], [12], [14], [20], [21], [29], [33], [40]. Recent researches devote to designing efficient network architectures and task-specific loss functions to enhance model performance. For instance, Dong et al. [5] exploited the multi-scale information of hazy images by designing a pyramid-like network. Guo et al. [8] propose a transformer-based network that utilizes 3D position embedding of the observed hazy image to achieve high-quality restoration. Wu et al. [40] proposed a novel contrastive regularization as the loss term to leverage connections among recovered images, hazy images and ground truth. Similarly, image deraining [30], [31] and desnowing [3], [23] aim to removal the effect of rain streak and snow from the degraded images. Most of them are focusing on developing task-specific network structure and loss function, and achieving promising results.

Instead of improving the restoration performance through designing novel network structure or loss function, this study shows another feasible but ignored way, i.e., introducing an auxiliary restoration task to improve the generalization of models. The proposed RQID solution enjoys following two highly-expected merits. On the one hand, it can be compatible to existing network and criterion, thereby enjoying high generalizability and flexibility. On the other hand, it is free from extra training costs, embracing computational efficiency.

III. Proposed Method

In this section, we will first elaborate on three fundamental design principles of RQID in Section III-A. Based on these principles, we introduce the DRI to quantify the degradation relationship in Section III-B. Next, Section III-C presents Degradation Proportion Determination strategy (DPD) to estimate whether given auxiliary degradations benefit the anchor degradation. Finally, we detail the construction process of the RESIDE+ in Section III-D.

A. Principles of Quantifying Degradation Relationship

RQID is an emerging topic in low-level vision with many aspects unexplored. To establish a robust and accurate quantification of the relationship, we present two fundamental guiding principles for method development: the asymmetric principle and content-irrelevant principle.

Asymmetric principle: Different from the symmetric similarity metrics, such as Euclidean distance and structure similarity, the degradation relationship should be asymmetric since RQID aims to measure the influence of the auxiliary degradation on the anchor task. Clearly, such a goal is asymmetric. In other words, a degradation combination is positive to the anchor restoration, which might be negative to the auxiliary restoration.

Content irrelevant principle: Another designing principle to RQID is content irrelevant, i.e., the RQID metric can avoid distraction of image content and only reflect degradation relationship. However, it is daunting even impossible to fully follow this principle in practice, since the degradations are coupled with contents. As a remedy, we conduct experiments on images that have the same image content but different degradation types. Considering degradation is the only difference among them, the quantification results could be regarded as approximately irrelevant to the content.

B. Degradation Relationship Index

As aforementioned, DRI quantifies the relationship between the anchor and the auxiliary degradations through the mean drop rate difference $\bar{D}$ in validation loss between two models, where one is trained solely on the anchor degradation and the other is trained on both two degradations. To be specific, for a given batch of training samples $\mathcal{X}^{1,2} = \{X^1, X^2\} = \{x_1^1, \cdots x_i^1, x_{i+1}^2, \cdots x_N^2\}$ with batch size N. X^1, X^2 and $\mathcal{X}^{1,2}$ denote samples with anchor degradation, auxiliary degradation, and both of them, respectively. Supposing we adopt stochastic gradient descent to update the model parameters θ^t, the update process can be expressed as:

$$\theta_{\mathcal{X}^{1,2}}^{t+1} = \theta^t - \eta \nabla \mathcal{L}(\mathcal{X}^{1,2}, \theta^t), \tag{1}$$

where η denotes the learning rate and $\theta_{\mathcal{X}^{1,2}}^{t+1}$ represents the model parameters at step $t+1$, updated by $\mathcal{X}^{1,2}$. Given the updated model $\theta_{\mathcal{X}^{1,2}}^{t+1}$, the validation loss with respect to validation samples X_v^1 can be computed as $\mathcal{L}(X_v^1, \theta_{\mathcal{X}^{1,2}}^{t+1})$. Similarly, let $\mathcal{X}^1 = \{x_1^1, \cdots x_N^1\}$ denote the training batch only containing the anchor degradation. The model parameters $\theta_{\mathcal{X}^1}^{t+1}$ is updated by $\mathcal{X}^1$ as follows:

$$\theta_{\mathcal{X}^1}^{t+1} = \theta^t - \eta \nabla \mathcal{L}(\mathcal{X}^1, \theta^t). \tag{2}$$

The corresponding validation loss with respect to X_v^1 is then given by $\mathcal{L}(X_v^1, \theta_{\mathcal{X}^1}^{t+1})$.

Based on the definitions above, let D_t denote the drop rate difference at time step t, it can be expressed as:

$$\begin{aligned} D_t &= \Phi(\mathcal{X}^1, X_v^1, t) - \Phi(\mathcal{X}^{1,2}, X_v^1, t) \\ &= \frac{\mathcal{L}(X_v^1, \theta_{\mathcal{X}^1}^{t+1}) - \mathcal{L}(X_v^1, \theta_{\mathcal{X}^{1,2}}^{t+1})}{\mathcal{L}(X_v^1, \theta^t)}, \end{aligned} \tag{3}$$

where $\Phi(\mathcal{X}^1, X_v^1, t)$ and $\Phi(\mathcal{X}^{1,2}, X_v^1, t)$ are the drop rates of validation loss for the two corresponding models.

To mitigate the volatility of the Drop Rate Difference (DRD), DRI is defined as the average of D_t. By default, this average is computed over the entire training process, expressed as

$$\bar{D} = \frac{1}{T} \sum_{t=1}^{T} D_t, \tag{4}$$

where T is the total number of training steps. Alternative sampling strategies for computing the average can be referred in the experimental part. According to the definition of DRI, a positive $\bar{D}$ indicates that the model trained with auxiliary degradation results in a higher drop rate compared to the one trained solely with the anchor degradation. In other words, a positive $\bar{D}$ suggests that the given degradation combination can enhance performance on the anchor restoration task.

C. Degradation Proportion Determination

Based on the observations in Fig. 1, which demonstrate that the proportion of auxiliary degradation influences the anchor restoration task, we employ DRI to further analyze this relationship. Specifically, we evaluate how the proportions of auxiliary degradation influence performance. As a case study, we utilize MSBDN [5], a representative image dehazing network, to examine the effect of auxiliary degradations (noise) on the anchor task (image dehazing). The proportions of auxiliary degradation p is varied from 0.1 to 0.9in increments of 0.2. From Table I, the following observations can be drawn: i) the proportion of degradation combinations plays a critical role in image restoration performance. Specifically, only certain proportions, such as 10% noise, benefit the anchor restoration task, while others deteriorate its performance; ii) DRI exhibits a strong correlation with performance on the anchor task. In brief, a positive DRI consistently indicates performance improvement

TABLE I
PERFORMANCES ON IMAGE DEHAZING WITH DIFFERENT PROPORTIONS OF AUXILIARY DEGRADATIONS (NOISE).

p	DRI	PSNR	Δ_{PSNR}	SSIM	Δ_{SSIM}
0%	0	33.84	-	0.9849	-
10%	**0.00090**	**33.96**	**0.12**	**0.9850**	**0.0001**
30%	-0.00301	33.00	-0.84	0.9828	-0.0021
50%	-0.01222	32.81	-1.03	0.9827	-0.0022
70%	-0.02784	32.10	-1.74	0.9804	-0.0045
90%	-0.05140	30.96	-2.88	0.9764	-0.0085

Results in boldface indicate the setting with best performance.

Algorithm 1: Degradation Proportion Determination.

Require: A given dataset $\mathcal{D}$, auxiliary degradation proportion p, network parameter θ, batch size N, maximal training step T.
for $t = 1$ to T **do**
Sample two mini-batches data $\mathcal{X}^1$, $\mathcal{X}^2$ from $\mathcal{D}$
Mix $\mathcal{X}^1$ and $\mathcal{X}^2$ with proportion p and obtain $\mathcal{X}^{1,2}$
Update the network parameter through (1) and 2 and get $\theta^{t+1}_{\mathcal{X}^{1,2}}, \theta^{t+1}_{\mathcal{X}^1}$.
Calculate D_t through (3).
end for
Calculate DRI via $\bar{D} = \frac{1}{T}\sum_{t=1}^{T} D_t$.
if $\bar{D} > 0$ **then**
Given degradation combination with proportion p, it would improve the performance on anchor restoration task.
else
Given degradation combination with proportion p, it would damage the performance on anchor restoration task.
end if

on anchor tasks, whereas a negative DRI suggests a decline in performance.

Based on these observations, we propose the Degradation Proportion Determination (DPD) strategy to optimize the performance of the anchor restoration task by identifying an appropriate auxiliary degradation proportion that ensures a positive DRI. The implementation details of DPD are summarized in Algorithm 1. DPD offers the following advantages. First, it is a time-saving strategy for estimating and determining whether a given proportion can enhance performance on the anchor restoration task. By reducing the sampling interval of DRI, the DPD could achieve $3.33\times$ speedup, resulting in high computational efficiency. Second, DPD exhibits strong interpretability, making its results explainable and reliable.

D. Benchmark

To mitigate the content discrepancy, benchmarks consisting of clean images paired with multiple degraded versions are highly desirable. Since no existing datasets fulfill these requirements, we extend the well-known image dehazing dataset, RESIDE [15], by synthesizing multiple degraded versions from its clean images for evaluation purposes. The resulting benchmark, termed RESIDE+, comprises 10,931 clean images along with their corresponding rainy, hazy and snowy versions. Detailed information about dataset construction and the synthesis process are provided in the supplementary materials.

IV. EXPERIMENTS

In this section, we aim to answer following questions: i) Can DRI predict performance changes across different anchor degradations? ii) Can conclusions derived from DRI be generalized across distinct backbones? iii) Can other task affinity methods effectively capture degradation relationships? To address these questions, we conduct a series of experiments to evaluate DRI's predictability across different degradation combinations, its robustness across different models, and the effectiveness of alternative task affinity approaches. Additionally, We include analysis experiments to further evaluate the impact of various factors on the performance of the proposed method.

A. Experimental Settings

In this section, we introduce the details of the dataset, baselines, evaluation metrics, and training details.

Dataset: In addition to aforementioned RESIDE+, we also evaluate our method on three additional real-world degraded datasets, including SPA [38] for deraining, Foggy Driving Dataset (FDD) [32] for dehazing, and Snow100K [23] for desnowing. Specifically, SPA consists of 1,000 real-world rainy images, FDD contains 101 hazy driving scene images, and Snow100 K includes 1,329 real-degraded snowy images collected from the Internet. Following [18], [45], we generate noisy images by adding white Gaussian noise to clean images with $\sigma = 15$.

Baselines: We take experiments on seven representative dehazing methods, including AOD-Net [14], GDN [21], FFANet [29], GCANet [1], MSBDN [5], AECR-Net [40] and Dehamer [8], to validate the generalizability of DRI.

Evaluation Metrics: Following [8], [14], [40], we adopt the Peak Signal-to-Noise Ratio (PSNR) [9] and the Structural SIMilarity (SSIM) [39] to measure image quality with the help of ground truth. Besides, two well-known No-Reference Image Quality Assessments (NRIQA), i.e., SSEQ [19] and NRQM [24], are adopted to evaluate the generalizability on real-degraded images. Pearson correlation coefficient (Pearson's coefficient) is adopted to measure linear correlation between DRI and final performance. Higher value of PSNR, SSIM, NRQM and Pearson's coefficient indicate better performance of methods, whereas lower SSEQ value represents better performance.

Training details: We conduct experiments in PyTorch on NVIDIA GeForce RTX 3090 GPUs. For fair comparisons, we use the officially released codes to train the networks if they are publicly available. Except for partial training samples are replaced by other degradations, all the experimental settings are the same as the official settings.

B. Validation of DRI's Predictability

To verify predictability of DRI, we retrain the MSBDN with different degradation combinations on both synthetic and real

TABLE II
QUANTITATIVE RESULTS OF DIFFERENT ANCHOR DEGRADATIONS ON THE SOTS+ DATASET.

Anchor Degradation	Metric	10% Haze	10% Rain	10% Snow	10% Noise
Haze	DRI	0	0.00879 ↑↑↑	0.00865 ↑↑	0.00860 ↑
	PSNR	33.84	34.76 ↑↑↑	34.50 ↑↑	33.96 ↑
	SSIM	0.9849	0.9857 ↑↑↑	0.9851 ↑↑	0.9850 ↑
	NRQM	8.25	8.28 ↑↑↑	8.28 ↑↑	8.26 ↑
	SSEQ	30.37	30.24 ↑↑↑	30.32 ↑↑	30.71 ↓
Rain	DRI	-0.04090 ↓↓↓	0	-0.00167 ↓	-0.00457 ↓↓
	PSNR	36.66 ↓↓↓	38.12	37.61 ↓	37.59 ↓↓
	SSIM	0.9587 ↓↓↓	0.9652	0.9635 ↓↓	0.9636 ↓
	NRQM	8.53 ↓↓↓	8.58	8.56 ↓	8.56 ↓↓
	SSEQ	11.21 ↑	12.58	13.02 ↓	13.46 ↓↓
Snow	DRI	-0.12649 ↓↓↓	-0.00234 ↓	0	0.00143 ↑
	PSNR	36.52 ↓↓↓	36.80 ↓	36.81	36.84 ↑
	SSIM	0.9768 ↓↓↓	0.9781 ↑↑	0.9778	0.9781 ↑
	NRQM	8.50 ↓↓↓	8.53 ↓	8.53	8.55 ↑
	SSEQ	13.67 ↓↓	13.49 ↓	13.06	14.41 ↓↓↓
Noise	DRI	-0.04845 ↓↓↓	-0.00097 ↓↓	0.00024 ↑	0
	PSNR	34.78 ↓↓↓	34.83 ↓	34.89 ↑	34.85
	SSIM	0.9457 ↓↓↓	0.9462 ↓↓	0.9470 ↑	0.9468
	NRQM	8.35 ↓↓↓	8.39 ↓↓	8.40 ↓	8.41
	SSEQ	23.45 ↓↓↓	21.63 ↓↓	20.50 ↑	20.82

A higher value of PSNR/SSIM/NRQM indicates better performance, while a lower value of SSEQ signifies better performance. ↑ indicates the degree of performance improvement, while the ↓ indicates the degree of performance decrement.

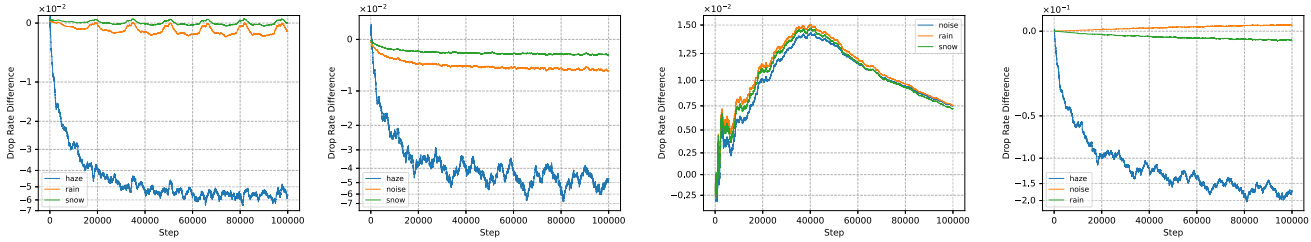

(a) Anchor degradation: **noise**. (b) Anchor degradation: **rain streak**. (c) Anchor degradation: **haze**. (d) Anchor degradation: **snow**.

Fig. 2. The DRD on four anchor degradations (i.e., noise, rain streak, haze, and snow) during the training stage. Different colors indicate different auxiliary degradations.

datasets to evaluate the connections between DRI and final performance.

1) Results on Synthetic Datasets: As shown in Table II, DRI demonstrates high predictability on synthetic datasets, where a positive DRI consistently indicates performance improvement on anchor tasks, and vice versa. Additionally, we analyze the behavior of DRD throughout the training process. As illustrated in Fig. 2, DRD displays noticeable fluctuations during training. For instance, as depicted in Fig. 2(a), even though the DRI for snow remains positive, DRD still exhibits occasionally negative values. These fluctuations highlight the inherent variability of DRD during training, further validating the reasonability behind DRI, which mitigates such variations by averaging DRD over multiple steps to provide a more stable and reliable performance metric.

2) Results on Real-Degraded Images: To verify the generalizability of DRI on real degradations, we conduct both qualitative and quantitative experiments on three representative real-degraded datasets, including SPA [38], FDD [32], and Snow100K [23]. As shown in Table III, DRI demonstrates strong generalizability on real-degraded images, indicating that DRI calculated on the synthetic datasets can reliably predict performance changes on the real-world images. For qualitative analysis, as illustrated in Fig. 3, models trained solely on hazy images produce artifacts on real hazy images, while models trained with positive auxiliary degradations, such as noise, rain streaks and snow, avoid such artifacts and generate clear and visually appealing outputs. Similar conclusions can be derived from Figs. 4, 5, where positive auxiliary degradations enhance performance in real-world scenarios, whereas negative degradations adversely affect performance.

C. Validation of DRI's Generalizability

Without loss of generality, we take haze as anchor degradation, noise, rain streak and snow as auxiliary degradations to verify whether conclusions drawn from MSBDN can generalize to other backbones. As shown in Table IV, improvements have been achieved across different backbones by introducing the positive auxiliary degradations, demonstrating strong generalizability on multiple backbones. Similar conclusions can be drawn from the visual results presented in Figs. 6

TABLE III
QUANTITATIVE RESULTS OF THE PROPOSED METHOD ON REAL-DEGRADED DATASETS.

Anchor Degradation	Metric	10% Haze	10% Rain	10% Snow	10% Noise
Haze	DRI	0	0.00879 ↑↑↑	0.00865 ↑↑	0.00860 ↑
	NRQM	7.13	7.17 ↑↑↑	7.16 ↑↑	7.14 ↑
	SSEQ	19.01	17.74 ↑↑↑	18.00 ↑↑	19.79 ↓
Rain	DRI	-0.04090 ↓↓↓	0	-0.00167 ↓	-0.00457 ↓↓
	NRQM	4.97 ↑↑↑	4.69	4.65 ↓	4.64 ↓↓
	SSEQ	40.47 ↑↑↑	45.40	45.99 ↓↓	45.82 ↓
Snow	DRI	-0.12649 ↓↓↓	-0.00234 ↓↓	0	0.00143 ↑
	NRQM	8.06 ↓↓↓	8.15 ↓↓	8.19	8.20 ↑
	SSEQ	29.37 ↓↓	29.45 ↓↓↓	29.30	29.28 ↑

A higher value of NRQM indicates better performance, while a lower value of SSEQ signifies better performance. ↑ indicates the degree of performance improvement, whereas the ↓ indicates the degree of performance decrement. One could observe that DRI exhibits strong predictability on real-degraded images, where a positive DRI indicates performance improvement, and vice versa.

TABLE IV
QUANTITATIVE RESULTS OF IMAGE DEHAZING ON SOTS DATASET, DEMONSTRATING THE GENERALIZABILITY OF DRI ACROSS DIFFERENT BACKBONES

Scenes	Method	Original		10% Noise		10% Rain		10% Snow	
		PSNR	SSIM	PSNR	SSIM	PSNR	SSIM	PSNR	SSIM
Indoor	AOD-Net [14]	19.54	0.8244	+0.19	+0.0099	+0.45	+0.0133	+0.28	+0.0066
	GDN [21]	32.16	0.9836	+0.14	+0.0007	+0.71	+0.0020	+0.51	+0.0007
	FFANet [29]	36.39	0.9886	+0.40	-0.0020	+0.57	+0.0007	+0.54	+0.0008
	GCANet [1]	30.08	0.9601	+0.45	+0.0024	+1.16	+0.0052	+0.64	+0.0047
	MSBDN [5]	32.72	0.9806	+1.76	+0.0031	+2.42	+0.0052	+1.81	+0.0052
	AECR-Net [40]	37.17	0.9901	+0.11	+0.0000	+0.02	+0.0001	+0.12	+0.0002
	Dehamer [8]	36.63	0.9881	+0.05	+0.0023	+0.24	+0.0010	+0.16	+0.0020
Outdoor	AOD-Net [14]	23.52	0.9183	+0.16	+0.0010	+0.65	+0.0037	+0.47	+0.0020
	GDN [21]	30.86	0.9819	+0.24	+0.0004	+0.43	+0.0016	+0.32	+0.0013
	FFANet [29]	33.38	0.9840	+0.52	+0.0002	+0.59	+0.0002	+0.71	+0.0007
	GCANet [1]	26.08	0.9614	+0.07	+0.0034	+1.15	+0.0017	+1.02	+0.0021
	MSBDN [5]	33.84	0.9849	+0.12	+0.0001	+0.92	+0.0008	+0.66	+0.0002
	AECR-Net [40]	33.52	0.9840	+0.24	+0.0009	+0.29	+0.0006	+0.62	+0.0013
	Dehamer [8]	35.18	0.9860	+0.25	+0.0000	+0.93	+0.0009	+0.70	+0.0009

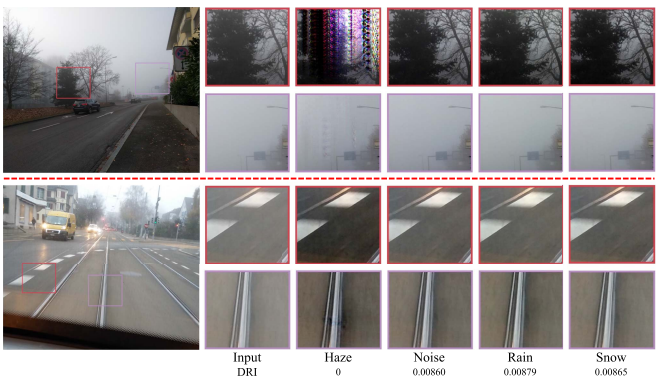

Fig. 3. Illustration of generalizability of DRI on real-world hazy images [32]. One could observe that DRIs calculated on synthetic datasets align with the performance changes on the real-world data, i.e., auxiliary degradations with positive DRI enhance the performance on anchor restoration tasks, and avoid the artifacts appeared in the baselines. Some areas are highlighted in rectangles and zooming-in is recommended for better visualizations and comparisons.

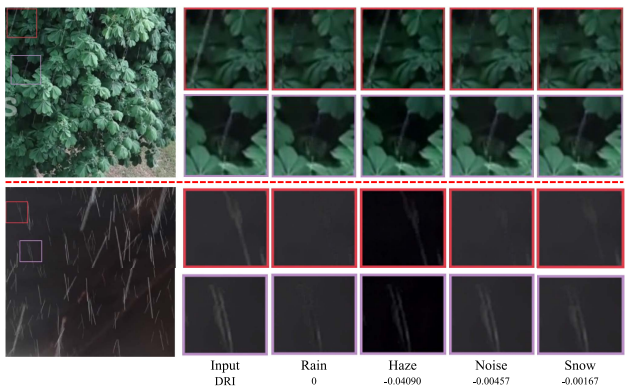

Fig. 4. Illustration of generalizability of DRI on real-world rainy images [38]. One could observe that DRI calculated on the synthetic datasets can reflect the performance changes on real-world datasets, i.e., auxiliary degradations with negative DRI adversely affect the results, remain more rain streaks than baselines. Some areas are highlighted in rectangles and zooming-in is recommended for better visualizations and comparisons.

and 7, where baselines trained with positive auxiliary degradations show better visual results and align more closely with the ground-truth, whereas original models often exhibit color distortions.

D. Comparison With Task Affinity Methods

In this section, we take haze as the anchor degradation, 10% noise, 10% rain, and 10% snow as the auxiliary degradation to make comparisons with two representative task

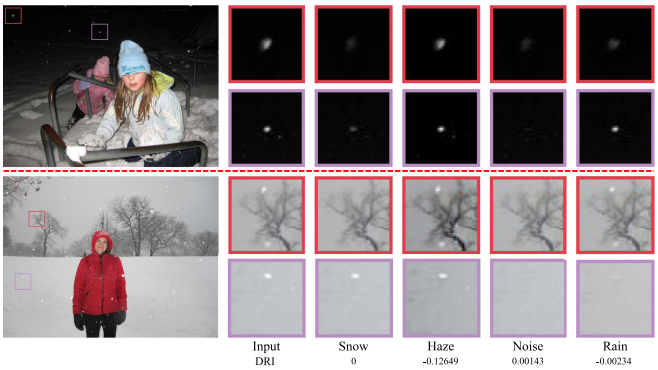

Fig. 5. Illustration of generalizability of DRI on real-world snowy images [23]. One could observe that DRI calculated on the synthetic datasets can reflect the performance changes on real-world datasets, i.e., auxiliary degradations with positive DRI results in clearer results, and vice versa. Some areas are highlighted in rectangles and zooming-in is recommended for better visualizations and comparisons.

TABLE V
THE DEGRADATION AFFINITY RESULTS OF DIFFERENT METRICS, INDICATING THE EFFECTIVENESS AND PREDICTABILITY OF DRI

Settings	Original	10% Noise	10% Rain	10% Snow
PSNR	33.84	33.96	34.76	34.50
SSIM	0.9849	0.9850	0.9857	0.9851
Taskonomy [42]	-	-1.00000	-0.00215	-0.000005
TAG [6]	-	-0.00189	-0.00060	-0.00142
DRI	-	0.00860	0.00879	0.00865

affinity methods, i.e., Taskonomy [42] and TAG [6]. As shown in Table V, our DRI demonstrates reliable predictability. Specifically, taking 10% noise as examples, the Taskonomy and TAG affinity are -1.00000 and -0.00189, respectively, which contradict the final performance on the anchor degradation. In contrast, the DRI is 0.00860, aligning with the observed performance improvement.

E. Analysis Experiments

In this section, we conduct further investigations on DRI. First, we compute DRI with different sampling steps to achieve better balance between performance and computational efficiency. Second, we calculate DRI with training loss to assess the necessity of validation loss. Additionally, experiments involving extra auxiliary degradations, proportions, degradation levels and multiple auxiliary degradations are conducted for further explorations. Finally, we present several intuitive explanations on auxiliary degradations.

1) Ablation Study on Sampling Steps: Calculating DRI at every iteration can be computationally expensive, making it essential to identify a balance that reduces computational overhead. Inspired by the results in Fig. 2, we observe that DRI values in consecutive steps are similar. This suggests that DRI can be computed at larger intervals rather than at every iteration, thereby saving time. To investigate this, we calculate DRI every 1, 5, 10, 50, 100 iterations, and evaluate its correlation with the final performance on anchor restoration tasks using Pearson's coefficient. Additionally, we also calculate DRI during the first, middle, and last 30% training steps to verify its predictability. As shown in Table VI, the results demonstrate that calculating DRI with larger intervals can accurately predict final performance. In other words, computing DRI over a limited subset of training steps, such as the first 30% steps, can yield reliable results.

TABLE VI
QUANTITATIVE RESULTS ON DIFFERENT SAMPLING STEPS.

Method	Pearson's Coefficient	Relative Speedup
Every 1 Step	0.9698	1.0×
Every 5 Steps	**0.9721**	1.93×
Every 10 Steps	0.9689	2.26×
Every 50 Steps	0.9586	2.45×
Every 100 Steps	0.9693	2.48×
First 30% Steps	0.9718	**3.33**×
Middle 30% Steps	0.9706	2.29×
Last 30% Steps	0.9674	1.73×

Speedup is relative to computing DRI in every 1 step. The best results on the pearson coefficient and the speedup are shown in boldface.

TABLE VII
PERFORMANCES ON IMAGE DEHAZING WITH DIFFERENT PROPORTIONS OF AUXILIARY TASK, I.E., IMAGE DENOISING.

p	DRI	PSNR	Δ_{PSNR}	SSIM	Δ_{SSIM}
0%	0	33.84	-	0.9849	-
1%	0.00132	33.86	0.02	0.9848	-0.0001
3%	0.00353	33.87	0.03	0.9851	0.0002
5%	0.00551	33.89	0.05	**0.9859**	**0.0010**
7%	0.00704	33.92	0.08	0.9853	0.0004
9%	0.00815	33.93	0.09	0.9853	0.0004
10%	**0.00860**	**33.96**	**0.12**	0.9850	0.0001
20%	0.00726	33.93	0.09	0.9857	0.0008

Results in boldface indicate the setting with best performance.

To further leverage above observations, we conduct time comparisons under following three settings. Namely, i) the traditional method: separately training two models for 100 K iterations, and comparing their results; ii) DPD-100 K: training a single model for 100 K iterations using DPD and measuring its DRI; and iii) DPD-30 K, training a single model for 30 K iterations using DPD and measuring its DRI. As illustrated in the results, the traditional method, DPD-100 K and DPD-30 K take 1726.20 mins, 1475.35 mins, and 492.03 mins, respectively. In other words, DPD-100 K and DPD-30 K saving 14.53% and 71.50% training time compared to the traditional method. These findings demonstrate a novel approach that can effectively balance time efficiency with performance, enabling DPD to achieve desired results with a significantly less time, thus offering a distinct advantage over traditional methods.

2) Ablation Study on Validation Loss: In this section, we investigate the necessity of validation loss in DRI by replacing it with training loss. As shown in Figs. 8 and 9, training loss fails to reflect the influence of auxiliary degradation. Specifically, as shown in Fig. 8, DRDs remain negative throughout the training process for a positive auxiliary degradation, contradicting the observations and results in Figs. Figs. 1, 10, and 11. Taking proportion of 0.1 as another example, 10% noise leads to performance improvement in Tables I and VII, while its DRI

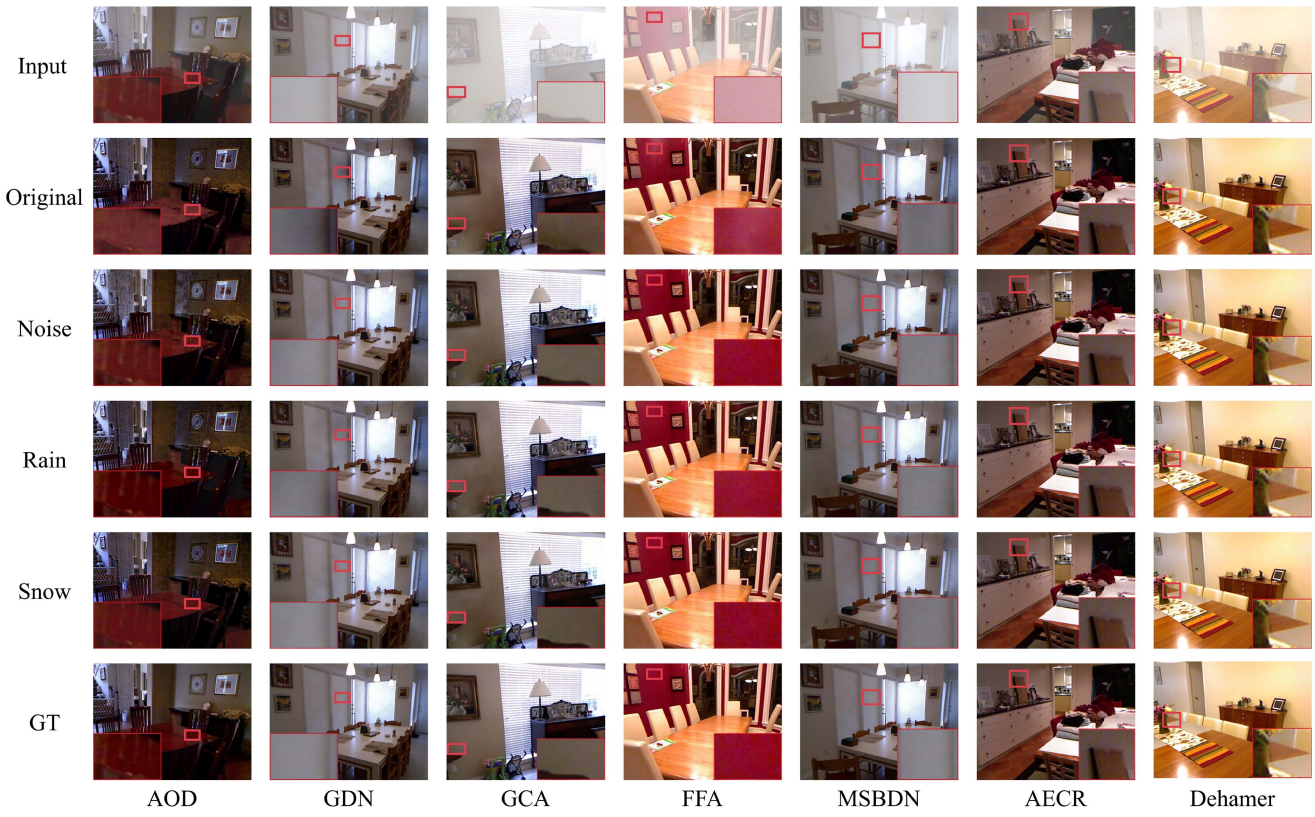

Fig. 6. Visual analysis on indoor scenes of SOTS dataset. Some areas are highlighted in red rectangles and zooming-in is recommended for better visualizations and comparisons. One could observe that models trained with positive auxiliary degradations show more visual pleasing results than baselines.

calculating by training loss is negative, highlighting the inadequacy of training loss. Similar conclusions could be derived from Fig. 9 as well. From above findings, we can find out that models trained without auxiliary degradations converge faster on the training set, while those trained with both anchor and positive auxiliary degradations achieve lower validation loss, indicating that appropriate auxiliary degradation improve generalizability of the model.

3) Results on Extra Auxiliary Degradations: We further examine the impact of masking, blurring, and color jitter on four anchor degradations, i.e., haze, noise, rain, and snow. As shown in Table VIII, following observations can be made: i) color jitter adversely affects the anchor tasks. Although Gaussian blur and masking exhibit marginal improvements in PSNR on some tasks (such as dehazing), they generally degrade the performance on most target restoration tasks. This phenomenon could be attributed to the severe color and structural distortions caused by these corruptions; ii) DRI demonstrates strong predictability in terms of PSNR. Specifically, the positive DRI correlates with PSNR improvements, while a negative DRI corresponds to performance degradation, which is consistent with our claims.

4) Analysis on Proportions of Auxiliary Degradations: We present additional results of extra auxiliary degradations' proportions and analyze the corresponding changes in DRD throughout the training process. As illustrated in Fig. 10, following observations can be made: i) DRI demonstrates strong predictability and can effectively reflect performance changes across different proportions; ii) 10% auxiliary degradation is optimal, and thus, to reduce computational costs, we adopt this proportion consistently in our experiments. Similar conclusions could be derived from Fig. 11.

TABLE VIII
RESULTS OF ADDITIONAL AUXILIARY DEGRADATIONS.

Anchor Degradation	Metric	Original	Color Jitter	Gaussian Blur	Mask
Haze	DRI	0	-0.00281	0.00756	0.00448
	PSNR	33.84	33.61	33.89	33.86
	SSIM	0.9849	0.9836	0.9849	0.9836
Rain	DRI	0	-0.03238	-0.00354	-0.06553
	PSNR	38.12	36.73	37.55	36.64
	SSIM	0.9652	0.9583	0.9624	0.9568
Snow	DRI	0	-0.04629	0.00086	-0.03137
	PSNR	36.81	36.52	36.84	36.57
	SSIM	0.9778	0.9769	0.9775	0.9764
Noise	DRI	0	-0.01970	-0.00002	-0.01362
	PSNR	34.85	34.79	34.85	34.81
	SSIM	0.9468	0.9452	0.9465	0.9464

The default proportions of auxiliary degradations are 10%.

5) Results on Multiple Auxiliary Degradations: We conduct additionally experiments on multiple auxiliary degradations in the following four settings, including two auxiliary degradations separately added to different images (dubbed as Two Degradation-Separate, 2D-S), two auxiliary degradations added to the same image (dubbed as Two Degradation-Joint, 2D-J),

Fig. 7. Visual analysis on outdoor scenes of SOTS dataset. Some areas are highlighted in red rectangles and zooming-in is recommended for better visualizations and comparisons. One could observe that models trained with positive auxiliary degradations show more visual pleasing results than baselines.

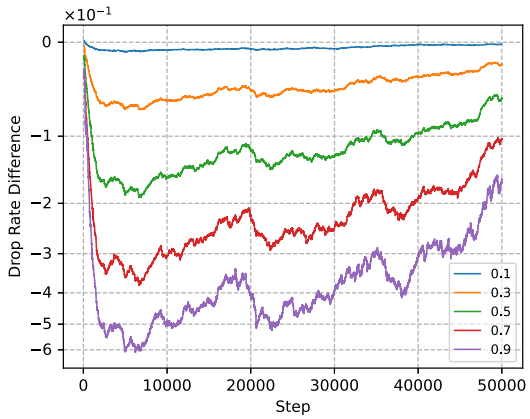

Fig. 8. DRD calculated on training loss during the training stage. Different colors indicate different proportions of auxiliary degradations.

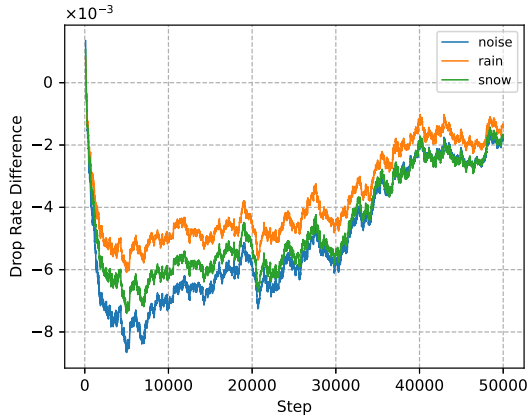

Fig. 9. DRD calculated on training loss with different degradation combinations during the training stage. Different colors indicate different auxiliary degradations.

three auxiliary degradations separately added to different images (dubbed as Three Degradation-Separate, 3D-S) and three auxiliary degradations added to the same image (dubbed as Three Degradation-Joint, 3D-J). As shown in Table IX, following two observations can be made. First, 2D-S and 3D-S achieved a compromise result. Taking "Rain & Noise" as the example, its performance is superior to the one using noise only but inferior to the one using rain only. This suggests that incorporating multiple degradations into different images will make the performance compromised by the weaker auxiliary degradation. Second, 2D-J and 3D-J achieve greater improvements compared to using single degradation, highlighting the benefits of combining multiple auxiliary degradations within the same image.

6) Results on Different Degradation Levels: To explore the impact of degradation levels, we conduct additional experiments by employing rain streaks as the anchor degradation and Gaussian noise with distinct noise levels ($\sigma = 10, 15, 25, 50$) as

TABLE IX
QUANTITATIVE RESULTS ON MULTIPLE AUXILIARY DEGRADATIONS.

Metric	Original	Single Degradation			2D-S			3D-S	2D-J			3D-J
		Noise	Rain	Snow	Rain&Noise	Rain&Snow	Snow&Noise	Rain&Snow&Noise	Rain+Noise	Rain+Snow	Snow+Noise	Rain+Snow+Noise
DRI	0	0.00860	0.00879	0.00865	0.00849	0.00826	0.00819	0.00816	0.00973	0.00919	0.00909	0.01011
PSNR	33.84	33.96	34.76	34.50	34.31	34.22	34.06	34.01	35.29	34.84	34.80	35.32
SSIM	0.9849	0.9850	0.9857	0.9851	0.9852	0.9842	0.9853	0.9856	0.9869	0.9860	0.9865	0.9860

2D-S (3D-S) denotes two (three) auxiliary degradations are separately added to different images. 2D-J (3D-J) denotes two (three) auxiliary degradations are added to the same image.

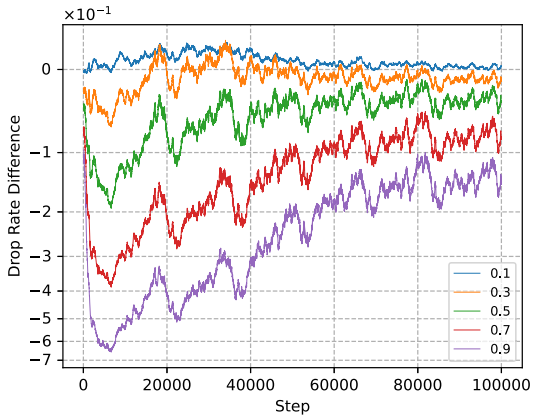

Fig. 10. The DRD on different proportions (ranging from 0.1 to 0.9) of auxiliary degradations, i.e., image denoising, during the training stages. As the proportion increases, the DRD decreases simultaneously.

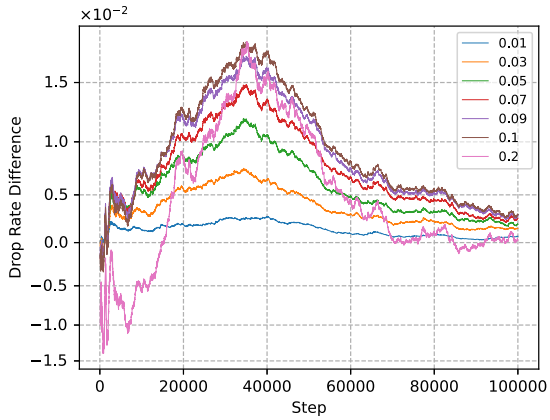

Fig. 11. The DRD on different proportions (ranging from 0.01 to 0.2) of auxiliary degradations during the training process. When the proportion is 0.1, the DRD reaches its highest value.

auxiliary degradations. As shown in Table X, the DRI values reveal a nearly negative correlation between noise level and deraining performance: higher noise level (such as $\sigma = 50$) result in more significant performance degradation compared to lower noise level (such as $\sigma = 15$). An exception is observed at $\sigma = 10$, where the DRI (-0.00481) and PSNR (36.90) deviate from the expected trend. Despite this discrepancy, DRI effectively reflects the performance changes, suggesting a unique interaction at this noise level and demonstrating that DRI can effectively reflect the performance changes across different degradation levels.

TABLE X
ANALYSIS EXPERIMENTS ON AUXILIARY DEGRADATIONS WITH DIFFERENT DEGRADATION LEVEL

σ	DRI	PSNR	Δ_{PSNR}	SSIM	Δ_{SSIM}
-	0	38.12	-	0.9652	-
10	-0.00481	36.90	-1.22	0.9587	-0.0066
15	-0.00457	37.59	-0.53	0.9636	-0.0016
25	-0.00537	36.73	-1.39	0.9576	-0.0076
50	-0.04116	36.31	-1.81	0.9550	-0.0102

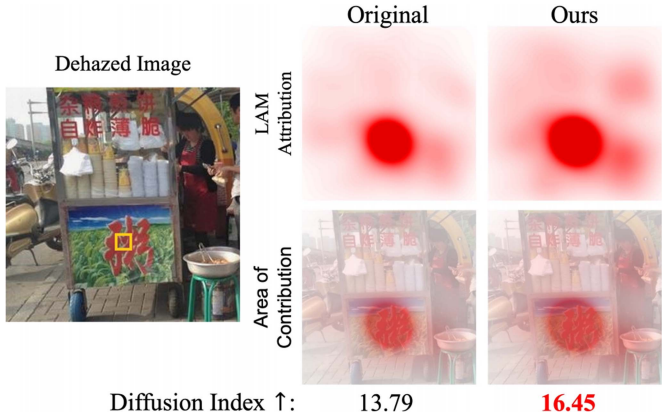

Fig. 12. LAM and DI for dehazing model interpretation.

7) Intuitive Explanation on Auxiliary Degradations: To intuitively illustrate the impact of auxiliary degradations on anchor task performance, we employ the Local Attribution Maps (LAM) [7] to visualize how the model utilizes pixel information from inputs to recover specific local regions. As shown in Fig. 12, it is evident that positive auxiliary degradation enable the network to leverage more information for recovery (see yellow rectangle). Additionally, the Diffusion Index (DI) [7], a metric quantifying the extent of input information utilized by the network, is introduced. A larger DI indicates more pixels are involved in the process. Our method outperforms original model, demonstrating that auxiliary degradations expand the influence areas of the network, thereby enhancing its recovery capability.

V. CONCLUSIONS AND LIMITATIONS

In this paper, we propose the Degradation Relationship Index (DRI) to quantify the degradation relationship by measuring the mean drop rate difference of validation loss between two models, where one trained solely with the anchor degradation and the other trained with the assistance of an auxiliary degradation.

Benefiting from DRI's ability to reflect the impact of auxiliary degradations on the anchor task, we can computationally identify potentially beneficial auxiliary degradations to enhance performance. Besides, a novel dataset, termed RESIDE+, is constructed to eliminate the content discrepancy and serve as a benchmark for this emerging research direction. Extensive experiments verify the effectiveness and generalizability of DRI.

However, as one of the first attempts to quantify degradation relationships, DRI exhibits several limitations. First, DRI exhibits inter-model variability in its quantitative values, preventing it from serving as a cross-model consistent performance indicator. Second, DRI quantifies degradation relationships on a pairwise basis, which may become inefficient as the number of potential degradations increases. To address these challenges, our future work will concentrate on i) developing cross-model consistent metrics through invariant feature normalization, enabling reliable performance prediction across different models, and ii) designing hierarchical computation frameworks to replace pairwise operations, achieving sub-linear complexity scaling for multi-degradation scenarios.

REFERENCES

[1] D. Chen et al., "Gated context aggregation network for image dehazing and deraining," in *Proc. IEEE Winter Conf. Appl. Comput. Vis.*, Waikoloa Village, HI, 2019, pp. 1375–1383.

[2] H. Chen et al., "Pre-trained image processing transformer," in *Proc. IEEE Conf. Comput. Vis. Pattern Recognit.*, 2021, pp. 12299–12310.

[3] W.-T. Chen et al., "ALL snow removed: Single image desnowing algorithm using hierarchical dual-tree complex wavelet representation and contradict channel loss," in *Proc. IEEE Int. Conf. Comput. Vis.*, Montreal, Canada, 2021, pp. 4176–4185.

[4] W.-T. Chen, Z.-K. Huang, C.-C. Tsai, H.-H. Yang, J.-J. Ding, and S.-Y. Kuo, "Learning multiple adverse weather removal via two-stage knowledge learning and multi-contrastive regularization: Toward a unified model," in *Proc. IEEE Conf. Comput. Vis. Pattern Recognit.*, New Orleans, LA, USA, 2022, pp. 17632–17641.

[5] H. Dong et al., "Multi-scale boosted dehazing network with dense feature fusion," in *Proc. IEEE Conf. Comput. Vis. Pattern Recognit.*, Seattle, WA, 2020, pp. 2154–2164.

[6] C. Fifty, E. Amid, Z. Zhao, T. Yu, R. Anil, and C. Finn, "Efficiently identifying task groupings for multi-task learning," in *Proc. Annu. Conf. Neural Inf. Process. Syst.*, 2021, pp. 27503–27516.

[7] J. Gu and C. Dong, "Interpreting super-resolution networks with local attribution maps," in *Proc. IEEE Conf. Comput. Vis. Pattern Recognit.*, 2021, pp. 9199–9208.

[8] C. Guo, Q. Yan, S. Anwar, R. Cong, W. Ren, and C. Li, "Image dehazing transformer with transmission-aware 3D position embedding," in *Proc. IEEE Conf. Comput. Vis. Pattern Recognit.*, New Orleans, LA, USA, 2022, pp. 5802–5810.

[9] Q. Huynh-Thu and M. Ghanbari, "Scope of validity of PSNR in image/video quality assessment," *Electron. Lett.*, vol. 44, no. 13, pp. 800–801, 2008.

[10] O. Kupyn, V.M. Budzan, M. Mykhailych, D. Mishkin, and J. Matas, "DeblurGAN: Blind motion deblurring using conditional adversarial networks," in *Proc. IEEE Conf. Comput. Vis. Pattern Recognit.*, Salt Lake City, UT, 2018, pp. 8183–8192.

[11] B. Li, Y. Gou, S. Gu, J. Z. Liu, J. T. Zhou, and X. Peng, "You only look yourself: Unsupervised and untrained single image dehazing neural network," *Int. J. Comput. Vis.*, vol. 129, no. 5, pp. 1754–1767, 2021.

[12] B. Li, Y. Gou, J. Z. Liu, H. Zhu, J. T. Zhou, and X. Peng, "Zero-shot image dehazing," *IEEE Trans. Image Process.*, vol. 29, pp. 8457–8466, 2020.

[13] B. Li, X. Liu, P. Hu, Z. Wu, J. Lv, and X. Peng, "All-in-One image restoration for unknown corruption," in *Proc. IEEE Conf. Comput. Vis. Pattern Recognit.*, New Orleans, LA, 2022, pp. 17431–17441.

[14] B. Li, X. Peng, Z. Wang, J. Xu, and D. Feng, "AOD-Net: All-in-one dehazing network," in *Proc. IEEE Int. Conf. Comput. Vis.*, Venice, Italy, 2017, pp. 4780–4788.

[15] B. Li et al., "Benchmarking single image dehazing and beyond," *IEEE Trans. Image Process.*, vol. 28, no. 1, pp. 492–505, Jan. 2019.

[16] R. Li, R. T. Tan, and L.-F. Cheong, "All in one bad weather removal using architectural search," in *Proc. IEEE Conf. Comput. Vis. Pattern Recognit.*, Seattle, WA, 2020, pp. 3172–3182.

[17] X. Li, J. Wu, Z. Lin, H. Liu, and H. Zha, "Recurrent squeeze-and-excitation context aggregation net for single image deraining," in *Proc. Eur. Conf. Comput. Vis.*, Munich, Germany, 2018, pp. 262–277.

[18] J. Liang, J. Cao, G. Sun, K. Zhang, L. Van Gool, and R. Timofte, "SwinIR: Image restoration using swin transformer," in *Proc. Int. Conf. Comput. Vis. Workshops*, Virtual, 2021, pp. 1833–1844.

[19] L. Liu, B. Liu, H. Huang, and A. C. Bovik, "No-reference image quality assessment based on spatial and spectral entropies," *Signal Process.: Image Commun.*, vol. 29, no. 8, pp. 856–863, 2014.

[20] R. Liu, S. Li, J. Liu, L. Ma, X. Fan, and Z. Luo, "Learning hadamard-product-propagation for image dehazing and beyond," *IEEE Trans. Circuits Syst. Video Technol.*, vol. 31, no. 4, pp. 1366–1379, Apr. 2021.

[21] X. Liu, Y. Ma, Z. Shi, and J. Chen, "GridDehazeNet: Attention-based multi-scale network for image dehazing," in *Proc. Int. Conf. Comput. Vis.*, Seoul, Korea, 2019, pp. 7313–7322.

[22] X. Liu, M. Suganuma, X. Luo, and T. Okatani, "Restoring images with unknown degradation factors by recurrent use of a multi-branch network," 2019, *arXiv:1907.04508*.

[23] Y.-F. Liu, D.-W. Jaw, S.-C. Huang, and J.-N. Hwang, "Desnownet: Context-aware deep network for snow removal," *IEEE Trans. Image Process.*, vol. 27, no. 6, pp. 3064–3073, Jun. 2018.

[24] C. Ma, C.-Y. Yang, X. Yang, and M.-H. Yang, "Learning a no-reference quality metric for single-image super-resolution," *Comput. Vis. Image Understanding*, vol. 158, pp. 1–16, 2017.

[25] P. Mu, Z. Liu, Y. Liu, R. Liu, and X. Fan, "Triple-level model inferred collaborative network architecture for video deraining," *IEEE Trans. Image Process.*, vol. 31, pp. 239–250, 2021.

[26] O. Özdenizci and R. Legenstein, "Restoring vision in adverse weather conditions with patch-based denoising diffusion models," *IEEE Trans. Pattern Anal. Mach. Intell.*, vol. 45, no. 8, pp. 10346–10357, Aug. 2023.

[27] J. Pan, R. Liu, Z. Su, and X. Gu, "Kernel estimation from salient structure for robust motion deblurring," *Signal Process.: Image Commun.*, vol. 28, no. 9, pp. 1156–1170 2013.

[28] P. W. Patil, S. Gupta, S. Rana, and S. Venkatesh, "Video restoration framework and its meta-adaptations to data-poor conditions," in *Proc. Eur. Conf. Comput. Vis.*, 2022, pp. 143–160.

[29] X. Qin, Z.Y. WangX. BaiXie, and H. Jia, "FFA-Net: Feature fusion attention network for single image dehazing," in *Proc. AAAI Conf. Artif. Intell.*, New York, NY, USA, 2020, pp. 11908–11915.

[30] D. Ren, W. Shang, P. Zhu, Q. Hu, D. Meng, and W. Zuo, "Single image deraining using bilateral recurrent network," *IEEE Trans. Image Process.*, vol. 29, pp. 6852–6863, 2020.

[31] D. Ren, W. Zuo, Q. Hu, P. Zhu, and D. Meng, "Progressive image deraining networks: A better and simpler baseline," in *Proc. IEEE Conf. Comput. Vis. Pattern Recognit.*, Long Beach, CA, USA, 2019, pp. 3932–3941.

[32] C. Sakaridis, D. Dai, and L. Van Gool, "Semantic foggy scene understanding with synthetic data," *Int. J. Comput. Vis.*, vol. 126, no. 9, pp. 973–992, Sep. 2018.

[33] Y. Song, Z. He, H. Qian, and X. Du, "Vision transformers for single image dehazing," *IEEE Trans. Image Process.*, vol. 32, pp. 1927–1941, 2023.

[34] S. Sun, W. Ren, X. Gao, R. Wang, and X. Cao, "Restoring images in adverse weather conditions via histogram transformer," in *Proc. Eur. Conf. Comput. Vis.*, 2025, pp. 111–129.

[35] Z. Tu et al., "Maxim: Multi-axis MLP for image processing," in *Proc. IEEE/CVF Conf. Comput. Vis. Pattern Recognit.*, 2022, pp. 5769–5780.

[36] J. M. J. Valanarasu, R. Yasarla, and V. M. Patel, "TransWeather: Transformer-based restoration of images degraded by adverse weather conditions," in *Proc. IEEE Conf. Comput. Vis. Pattern Recognit.*, New Orleans, LA, 2022, pp. 2343–2353.

[37] D. Wang, H. Tang, J. Pan, and J. Tang, "Learning a tree-structured channel-wise refinement network for efficient image deraining," in *Proc. IEEE Int. Conf. Multimedia Expo*, Shenzhen, China, 2021, pp. 1–6.

[38] T. Wang, X. Yang, K. Xu, S. Chen, Q. Zhang, and R. W. H. Lau, "Spatial attentive single-image deraining with a high quality real rain dataset," in *Proc. IEEE Conf. Comput. Vis. Pattern Recognit.*, 2019, pp. 12262–12271.

[39] Z. Wang, A. C. Bovik, H. R. Sheikh, and E. P. Simoncelli, "Image quality assessment: From error visibility to structural similarity," *IEEE Trans. Image Process.*, vol. 13, no. 4, pp. 600–612, Apr. 2004.

[40] H. Wu et al., "Contrastive learning for compact single image dehazing," in *Proc. IEEE Conf. Comput. Vis. Pattern Recognit.*, 2021, pp. 10551–105.

[41] W. Yang, R. T. Tan, J. Feng, Z. Guo, S. Yan, and J. Liu, "Joint rain detection and removal from a single image with contextualized deep networks," *IEEE Trans. Pattern Anal. Mach. Intell.*, vol. 42, no. 6, pp. 1377–1393, Jun. 2020.
[42] A. Zamir, A. Sax, W. Shen, L. Guibas, J. Malik, and S. Savarese, "Taskonomy: Disentangling task transfer learning," in *Proc. IEEE Conf. Comput. Vis. Pattern Recognit.*, Salt Lake City, USA, 2018, pp. 6241–6245.
[43] S.W. Zamir, A.S. AroraM. KhanF. HayatS. Khan, and M.-H. Yang, "Restormer: Efficient transformer for high-resolution image restoration," in *Proc. IEEE Conf. Comput. Vis. Pattern Recognit.*, New Orleans, LA, 2022, pp. 5718–5729.
[44] S.W. Zamir et al., "Multi-stage progressive image restoration," in *Proc. IEEE Conf. Comput. Vis. Pattern Recognit.*, 2021, pp. 14821–14831.
[45] K. Zhang, W. Zuo, Y. Chen, D. Meng, and L. Zhang, "Beyond a Gaussian denoiser: Residual learning of deep CNN for image denoising," *IEEE Trans. Image Process.*, vol. 26, no. 7, pp. 3142–3155, Jul. 2017.
[46] Y. Zhang, K. Li, K. Li, G. Sun, Y. Kong, and Y. Fu, "Accurate and fast image denoising via attention guided scaling," *IEEE Trans. Image Process.*, vol. 30, pp. 6255–6265, 2021.
[47] Y. Zhang, K. Li, K. Li, B. Zhong, and Y. Fu, "Residual non-local attention networks for image restoration," in *Proc. Int. Conf. Learn. Representations*, New Orleans, LA, 2019.
[48] Y. Zhang, Y. Tian, Y. Kong, B. Zhong, and Y. Fu, "Residual dense network for image restoration," *IEEE Trans. Pattern Anal. Mach. Intell.*, vol. 43, no. 7, pp. 2480–2495, Jul. 2021.
[49] R. Zhu, Z. Tu, J. Liu, A. C. Bovik, and Y. Fan, "MWFormer: Multi-weather image restoration using degradation-aware transformers," *IEEE Trans. Image Process.*, vol. 33, pp. 6790–6805, 2024.

Boyun Li received the BE degree in computer science and technology from Sichuan University, Chengdu, China, in 2019. He is currently working toward the PhD degree in computer science with the College of Computer Science, Sichuan University. His research interests include image restoration and machine learning.

Yuanbiao Gou received the BE degree from the School of Software Engineering, Sichuan University, Chengdu, China, in 2019. He is currently working toward the PhD degree with the School of Computer Science, Sichuan University. His current research interest includes image processing.

Wenxin Wang received the bachelor's degree in computer science and technology from Sichuan University, Chengdu, China, in 2022. He is currently working toward the master's degree in computer science with the College of Computer Science, Sichuan University. His research interest includes image restoration.

Peng Hu received the PhD degree in computer science and technology from Sichuan University, China, in 2019. He is currently an associate researcher with the College of Computer Science, Sichuan University. From 2019 to 2020, he was a research scientist with Institute for Infocomm, Research Agency for Science, Technology, and Research (A∗STAR) Singapore. His current interests mainly include focus on multi-view learning, cross-modal retrieval, and network compression.

Wangmeng Zuo received the PhD degree in computer application technology from the Harbin Institute of Technology, Harbin, China, in 2007. He is currently a professor with the School of Computer Science and Technology, Harbin Institute of Technology. He has published more than 100 papers in top-tier academic journals and conferences. According to the statistics by Google scholar, his publications have been cited more than 60,000 times in literature. His current research interests include image enhancement and restoration, image and face editing, object detection, visual tracking, and image classification. He has served as an associate editor for *IEEE Transactions on Image Processing*.

Xi Peng is currently a full professor with the College of Computer Science, Sichuan University. His current research interests include machine intelligence and has authored more than 50 articles in these areas. He has served as an associate editor/guest editor for six journals including *IEEE Trans on SMC: Systems* and *IEEE Transaction on Neural Network and Learning Systems*; an Area Chair/Senior Program Committee member for the conferences, such as IJCAI, AAAI, and ICME.